Journal of
Marine Science and Engineering

MDPI

Article

Free-Drop Experimental and Simulation Study on the Ultimate Bearing Capacity of Stiffened Plates with Different Stiffnesses under Slamming Loads

Jinsong Xia [1,2], Zhanyang Chen [3,4,*], Nan Zhao [1,2], Weidong Zhao [3,4], Qin Tang [5] and Shijian Cai [6]

1 China Ship Scientific Research Center, Wuxi 214082, China; xjs@cssrc.com.cn (J.X.); zhaonan702@126.com (N.Z.)
2 National Key Laboratory of Ship Structural Safety, Wuxi 214082, China
3 Department of Ocean Engineering, Harbin Institute of Technology at Weihai, Weihai 264209, China; weidong.zhao@hit.edu.cn
4 State Key Laboratory of Structural Analysis, Optimization and CAE Software for Industrial Equipment, Dalian University of Technology, Dalian 116024, China
5 School of Foreign Studies, Jiangnan University, Wuxi 214122, China; 8353510219@jiangnan.edu.cn
6 Marine Design & Research Institute of China, Shanghai 200011, China; caishijian@maric.com.cn
* Correspondence: chenzhanyang@hit.edu.cn; Tel.: +86-135-0631-8766

Abstract: Differing from previous studies on free-drop tests, this study focuses on the ultimate bearing capacity and failure mechanism of the ship's bow under slamming loads. A prototype ship's bow is selected to design two simplified stiffened plates with different stiffeners, and the lateral slamming loads used are equivalent to flare slamming loads. Free-drop tests of the two simplified models are conducted, and the test setups and procedures are provided. The experimental results of slamming pressures and structural responses are obtained. By comparing with the simulation results obtained by Arbitrary Lagrangian-Eulerian (ALE) fluid–structure coupling, the convergence study, symmetry, and independence verifications are carried out. Finally, the dynamic ultimate bearing capacity of stiffened plates with different stiffnesses under lateral slamming loads is studied. The results show that stiffeners enhance the ability of stiffened plates to resist plastic deformation under slamming loads, and T-section stiffeners can provide greater resistance to plastic deformation than other types.

Keywords: free-drop model test; lateral slamming load; ALE fluid–structure coupling; ultimate bearing capacity; stiffened plate

check for updates

Citation: Xia, J.; Chen, Z.; Zhao, N.; Zhao, W.; Tang, Q.; Cai, S. Free-Drop Experimental and Simulation Study on the Ultimate Bearing Capacity of Stiffened Plates with Different Stiffnesses under Slamming Loads. *J. Mar. Sci. Eng.* **2024**, *12*, 1291. https://doi.org/10.3390/jmse12081291

Academic Editor: Joško Parunov

Received: 3 July 2024
Revised: 25 July 2024
Accepted: 30 July 2024
Published: 31 July 2024

Copyright: © 2024 by the authors. Licensee MDPI, Basel, Switzerland. This article is an open access article distributed under the terms and conditions of the Creative Commons Attribution (CC BY) license (https://creativecommons.org/licenses/by/4.0/).

1. Introduction

When a ship navigates under severe sea conditions, the slamming phenomenon resulting from the violent impact between waves and the ship's hull can cause serious structural damage, particularly to the bow [1,2]. When the ship is subjected to slamming loads, its overall bearing capacity decreases and may even be completely lost, leading to shipwrecks, which constitute a significant proportion of maritime accidents each year [1–3]. As a dynamic load, the slamming action cannot be equated to a static load due to its extremely short duration. The magnitude of the slamming load can sometimes be several times that of the static load, or even several times the wave bending moment, subjecting the ship's bow to high slamming pressures. These pressures often cause deformation or damage to the hull structure and lead to greater longitudinal bending moments in the ship. Severe impacts can not only generate immense pressure but also cause irreversible damage or complete destruction to local structures [4–6].

Compared to dynamic analysis, the static method is more commonly used in many engineering fields due to its higher computational efficiency. Thus, many studies on the ultimate strength of the ship's hull for safety evaluations have been conducted using static

methods [7–10]. However, slamming is a strong nonlinear event, and it is necessary to carry out dynamic analysis for the strength of ships. Not much work or articles about experiments on the dynamic ultimate bearing capacity of structures under slamming loads have been reported. Therefore, it is essential to conduct in-depth studies on the dynamic responses and ultimate bearing capacity of the bow structure under slamming loads.

Moreover, as a highly nonlinear phenomenon, the temporal and spatial distribution characteristics of slamming pressure on the structural surface are related to many factors, such as the water entry velocity, geometric surface of the structure, elasticity of the structure, and air layers, making it challenging to fully describe using mathematical models. Thus, it is necessary to conduct experimental analysis on slamming behavior. Currently, the most commonly used methods for wave load and slamming issues are the "segmented model test" [11–14] and the "free-drop slamming test".

Compared to segmented model tests, the advantage of drop tests for slamming is that they focus more on the slamming mechanism, eliminating the interference from external factors such as waves and the ship model's navigation. Drop tests are usually conducted in towing tanks, targeting local structures. The structure impacts the still water surface in a free-fall state, and by measuring physical quantities such as slamming pressure, water entry velocity, and time of water entry, the test can predict design values or analyze the temporal and spatial distribution of slamming pressure. Based on this, many scholars have conducted numerous free-drop or controlled-speed drop tests on flat plates [15], V-shaped wedges [16], or typical wedge plate structures [17,18]. Moreover, in recent years, free-drop tests have also been conducted on the local structures of high-performance ships, such as the bow and cross-deck of trimarans. Wang et al. [19] conducted free-drop tests of two trimaran sections impacting still water to study the cross-deck slamming loads. By comparing the variation in flow field of the two models during the process of water entry, it was shown that the flow fields around the cross-decks of the two models were different. Li et al. [20] investigated the characteristics of wet deck slamming loads on a generic trimaran section through a series of free-drop slamming tests. Based on a weakening main hull method, a modified model was designed and tested to study the effect of the main hull profile on wet deck slamming. Duan et al. [21] carried out free-drop slamming tests of a trimaran section with different drop heights and heel angles to study the slamming characteristics, flow field, and trimaran motion in the process of water entry. The results showed the good symmetry and repeatability of the model test.

Most of the drop tests mentioned in the literature focus on studying the characteristics of slamming pressure, such as maximum slamming force, temporal and spatial distribution models of slamming force, and selection of slamming coefficients. However, there is still limited research on the plastic deformation and ultimate bearing capacity of structures under slamming loads due to limitations in experimental conditions and experimental cost.

Therefore, to achieve free-drop tests for the bearing capacity of structures, a certain ship's bow is simplified into two sets of wedge grillage with a water entry angle of 15°, thereby achieving the equivalence of flare slamming with lateral slamming loads. The rest of the paper is organized as follows. In Section 2, the test system, test model, data acquisition system, and test program are described in detail. The ALE fluid–structure coupling simulation is conducted in Section 3, including the model establishment, parameter setting and data presentation. In Section 4, a verification study of the repeatability, linear regression and independence of the different model for the test is conducted. The main results of the free-drop tests are presented in Section 5, focusing on the plastic deformation and ultimate bearing capacity. Moreover, the influence of different models on the failure mechanism is discussed. Finally, conclusions are drawn, and an outlook for future work is presented in Section 6.

2. Experimental Setup

The primary objective of this experiment is to conduct model tests on the dynamic ultimate bearing capacity of stiffened plates with different stiffness levels under lateral

slamming loads using a free-drop test approach. By measuring the slamming pressure, structural strain, and plastic deformation of the plates, the load characteristics and failure mechanisms of the stiffened plates are determined under lateral slamming loads.

2.1. Model Design

Considering the magnitude of the dynamic ultimate strength of stiffened plates and the experimental conditions, the grillage structure of a ship's bow is simplified by ignoring the curvature of the outer plate, and the four simplified stiffened plate models with different specifications are designed, including two non-stiffened plates, one stiffened plate with angled steel, and one stiffened plate with a T-section stiffener. The geometric parameters are shown in Table 1. #1 and #2 are non-stiffened plates with different thicknesses, and #3 and #4 are stiffened plates with different longitudinal stiffeners. Considering that a small water entry angle might cause cushion effects, the water entry angle for all experimental models is set to 15°. The material for the models is ordinary steel (Q235), which is widely used in many industrial fields. The density is 7850 kg/m^3, the elastic modulus is 2.1 × 10^{11} Pa, the yield strength is 235 MPa and the Poisson's ratio is 0.3. The steel sheets selected are hot-rolled.

The primary purpose of this experiment is to study the ultimate bearing capacity of stiffened plates under lateral slamming loads, which is a destructive test. The experimental models and sectional view are shown in Figure 1. Model 1 is comprises #1 and #3, and Model 2 comprises #2 and # 4. The total height of the stiffened plate and box structure models is 1000 mm, and the self-weight of the experimental model is approximately 750 kg (excluding ballast). The average draft of each model is around 0.5 m, and the height of the center of gravity is around 0.7 m. To prevent splashes from entering the box after water entry, a 0.4 m high splash guard is added to the top of the box during fabrication, which also enhances the sinking resistance of the entire experimental model.

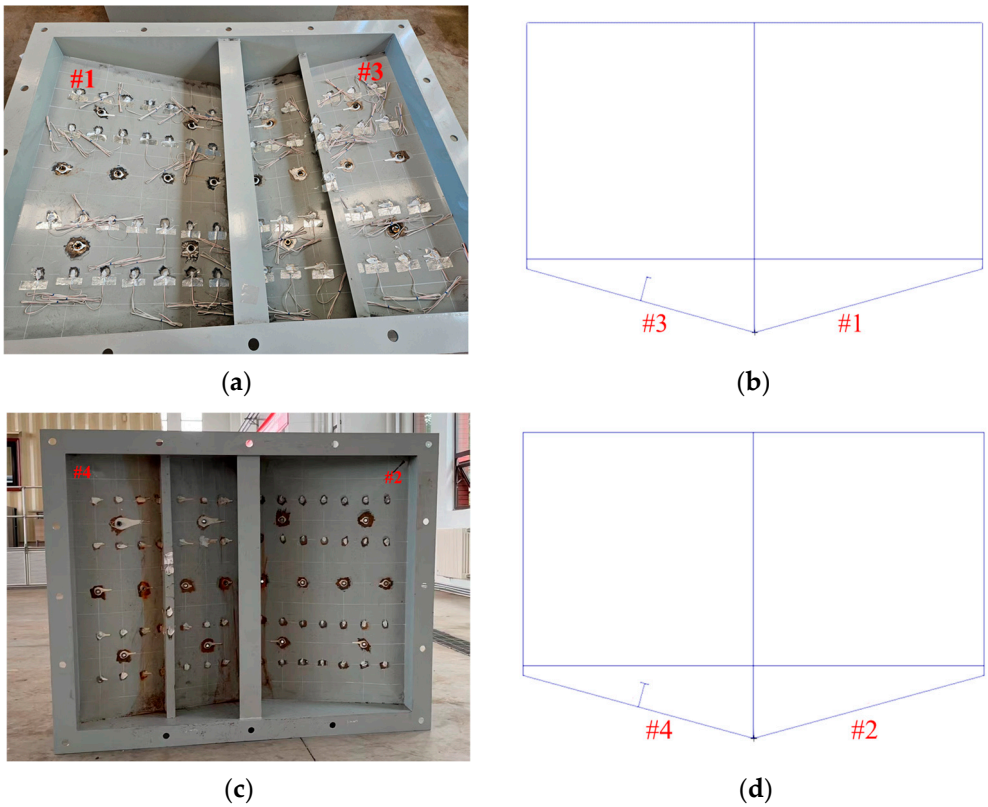

Figure 1. View of model: (**a**) Model 1 for test; (**b**) Diagram of Model 1; (**c**) Model 2 for test; (**d**) Diagram of Model 2.

Table 1. Structural parameters of stiffened plates.

No.	Length (mm)	Width (mm)	Thickness (mm)	Number of Stiffeners	Height of Web (mm)	Thickness of Web (mm)	Width of Plate (mm)	Thickness of Plate (mm)
#1 (Non-stiffened)	1200	800	2	0	--	--	--	--
#2 (Non-stiffened)	1200	800	3	0	--	--	--	--
#3 (Angled steel)	1200	800	2	1	100	2	20	3
#4 (T-section stiffener)	1200	800	2	1	100	2	40	3

2.2. Instruments

The experiment was conducted in the towing tank at the Qingdao Branch of China Ship Scientific Research Center, with a total depth of 10–12 m and an adjustable water surface height. The lifting device is 9 m above the ground. To ensure that the model falls in a normal state (with the bottom of the model level), the lifting device is used several times before the experiment to find the model's center of gravity, and the center of gravity is adjusted to the mid-longitudinal plane through weighting. During the experiment, the model is hoisted by the carriage, with a release device between the hook and the steel cable. To stabilize the model during the test, two traction ropes are attached to both ends longitudinally to adjust the model's position. In addition, a rope is attached to the lifting shackle, with its length adjusted to ensure that the steel mold does not accidentally sink and to facilitate lifting the steel cable after the model enters the water. The release process is completed using a wireless remote control to open the release device. The suspension setup for the experimental model is shown in Figure 2.

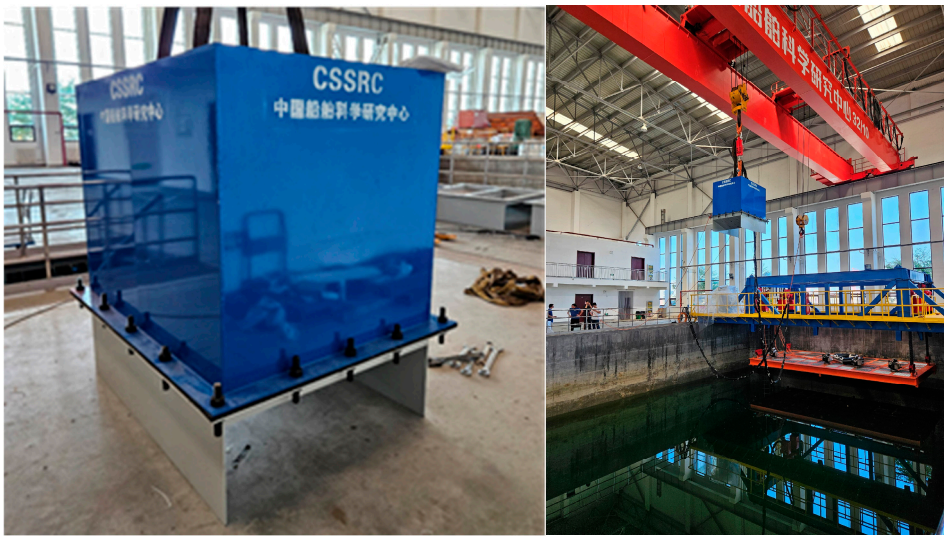

Figure 2. Suspension device for the experimental model.

In this study, the measured data acquired from the experimental procedure mainly include the slamming pressure and structural strain, which are measured by the pressure sensors and strain sensors, respectively. The pressure sensors used in the experiment have a range of 500 kPa to 1 MPa, and the accelerometers have a range of 5 g. The strain sensors are unidirectional strain gauges. Data acquisition systems are used to collect measurement data. All instruments and sensors are in good condition and within their calibration validity period. The wiring and instrument layout of the experimental model are shown in Figure 3a,b. Before and after the test, structural deformation measurements of the experimental model are taken using the scanner, as shown in Figure 3c.



(**a**) (**b**) (**c**)

Figure 3. Main test equipment: (**a**) Wiring of experimental model; (**b**) Data acquisition instruments; (**c**) Structural deformation scanner.

2.3. Test Conditions and Content

It is well known that the slamming pressure depends on the water entry velocity of the structure [22,23]. This experiment ensures that the model reaches the rated water entry velocity by adjusting the drop height. The drop height is defined as the distance from the lowest point of the model to the water surface. The model is lifted by the lifting device, and the height of the model from the ground can be measured by using a laser range finder at the edge of the towing tank. Since the distance between the still water and the ground is fixed, the distance between the model and the still water, which is the drop height, can be obtained. The experiment includes five different drop heights: 1.0 m, 1.5 m, 2.5 m, 5.1 m, and 7.34 m. The drop heights at which the two models respectively reached the plastic deformation are 5.1 m and 7.34 m. The specific conditions are presented in Table 2.

Table 2. Simulation conditions.

Model	Case	Water Entry Angle (deg)	Drop Height (m)	Water Entry Velocity (m/s)
1	1	15	1.00	4.43
	2	15	1.50	5.42
	3	15	2.50	7.00
	4 (Structure failure)	15	5.10	10.00
2	5	15	5.10	10.00
	6 (Structure failure)	15	7.34	12.00

3. Numerical Simulation

In this study, the ALE fluid–structure coupling method available in commercial LS-DYNA software is used to study the water entry of elastic stiffened plates [19,20]. To compare the simulation results with the experimental results, considering the high-frequency characteristics of the slamming pressure, the sampling frequency for the simulation is 2 kHz. Additionally, to save computational resources, the model's drop height is shortened in the simulation, only ensuring that the model meets the water entry velocity.

3.1. Simulation Model and Parameters

The simulation model of the upper box structure is shown in Figure 4a, which is set as a rigid body to reduce the simulation time. The stiffened plate models, which are made of elasto-plastic materials, are presented in Figure 4b,c. In this study, the wedge grillage is a thin shell structure modeled using the quadrilateral mesh. After verification of grid

independence (as shown in Section 4.1), the mesh size of each wedge grillage is determined to be 20 mm × 20 mm. The total mesh number of the wedge grillage is 33,312.

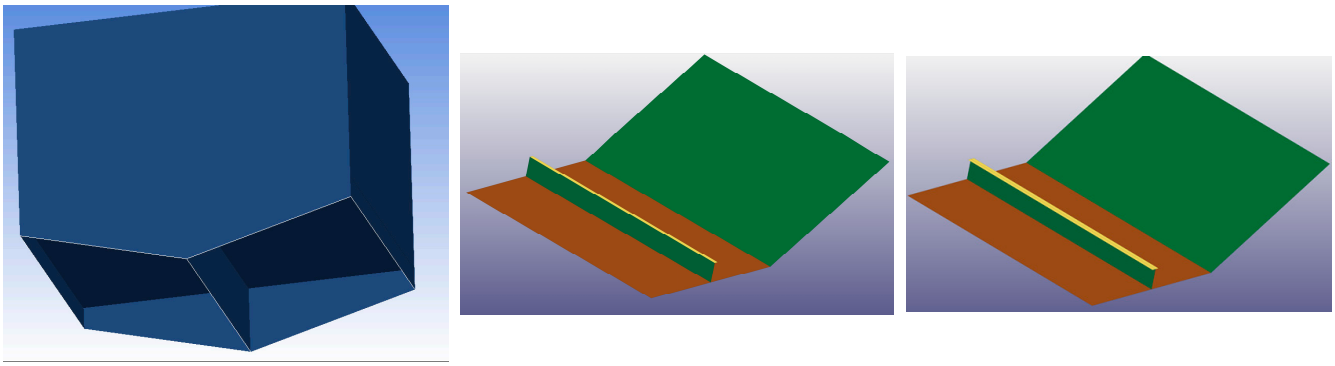

(**a**) (**b**) (**c**)

Figure 4. Simulation structural model: (**a**) Upper box model; (**b**) Angled steel stiffened plate (#1 and #3); (**c**) T-bar stiffened plate (#2 and #4).

In addition to the wedge model, the ALE method also requires constructing a fluid domain model, including the air domain and the water domain. The dimensions of the water domain are 4.5 m × 2.4 m × 1.25 m, and the air domain dimensions are also 4.5 m × 2.4 m × 1.25 m. To ensure computational accuracy and reduce the computation time, the fluid domain model is meshed with a gradient grid, with refined grids in the middle and coarse grids around the edges. The total mesh number of fluid domain is 883,200.

Furthermore, during the simulation, the reference atmospheric pressure is applied at the boundaries of the fluid domain rather than the entire fluid. The gravity acceleration of 9.81 kN/m^2 is applied vertically downward to all boundary layers, along with a reference atmospheric pressure of 1.013 × 10^5 Pa. The water entry of the simulation model is presented in Figure 5.

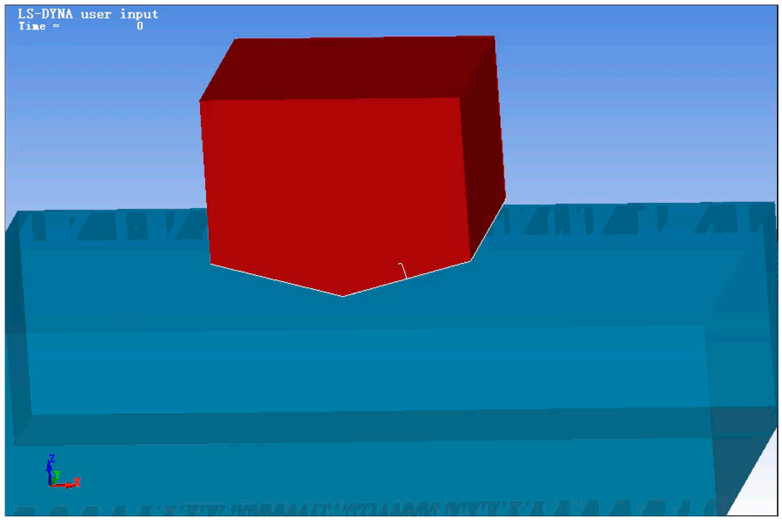

Figure 5. Water entry of simulation model.

3.2. Monitoring Points and Data Presentation

The simulation study corresponds with the experiment, and the arrangement of monitoring points are presented in Figure 6. Each stiffened plate has 8 pressure monitoring points (denoted by P) and 32 strain monitoring points (denoted by S). S15/16 and S17/18 indicate one strain gauge on the web and one on the panel of the stiffener, respectively.

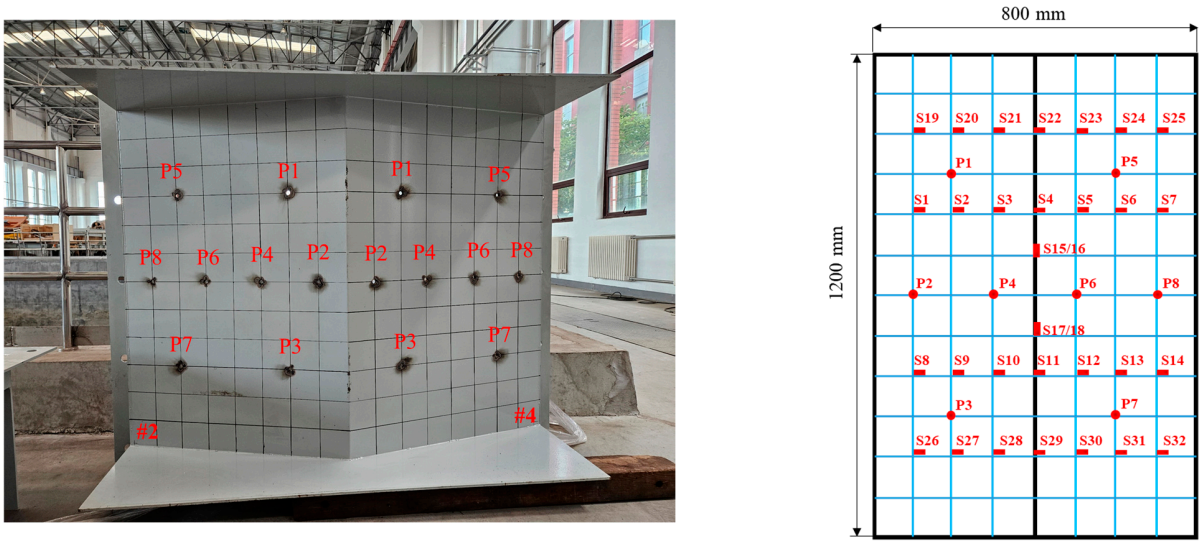

(**a**) (**b**)

Figure 6. Arrangement of pressure monitoring points of Model 2: (**a**) Test model; (**b**) Pressure and strain monitoring points for #4.

The time series of slamming pressure of Model 1 in Case 4 are presented in Figure 7. It can be seen that slamming occurs around 0.1 s, and the higher the entry point, the lower the water entry velocity and pressure. The pressure values at the same vertical height are almost equal.

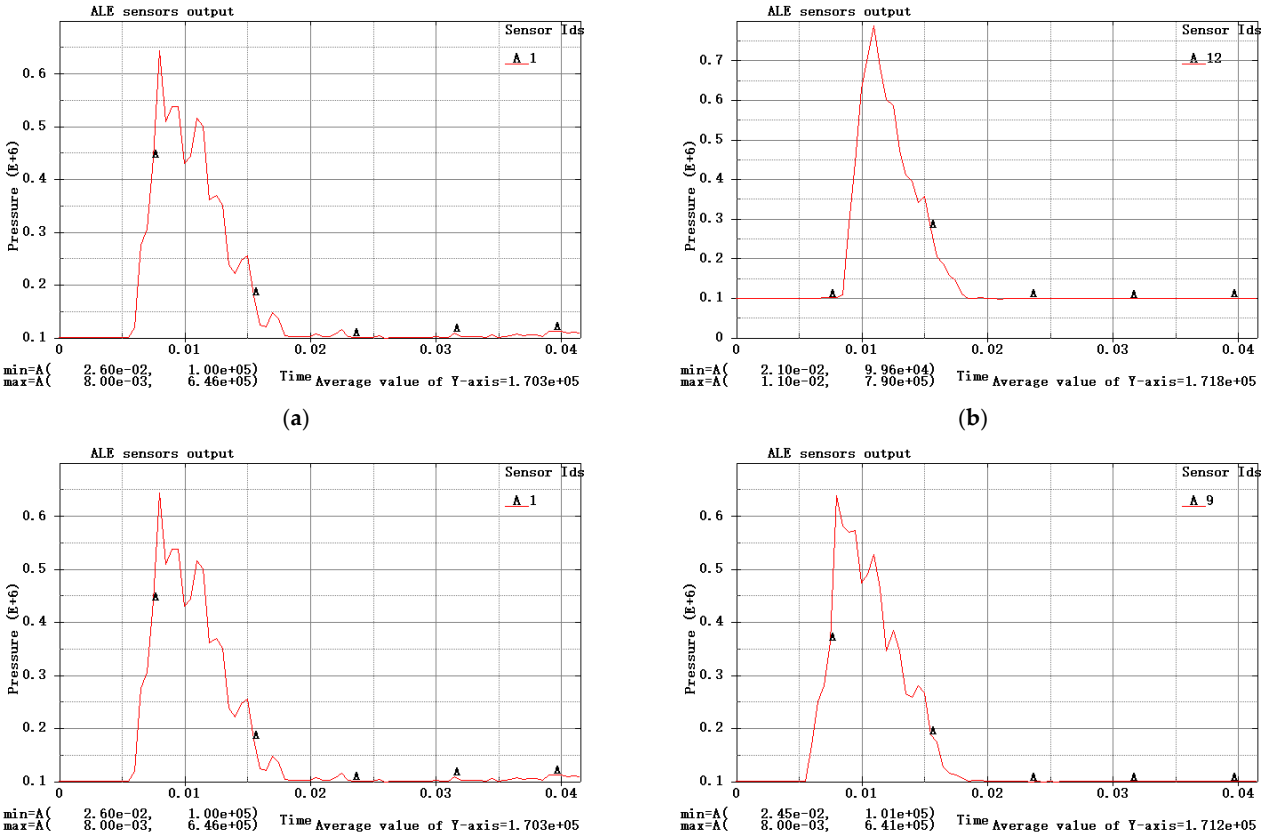

Figure 7. *Cont.*

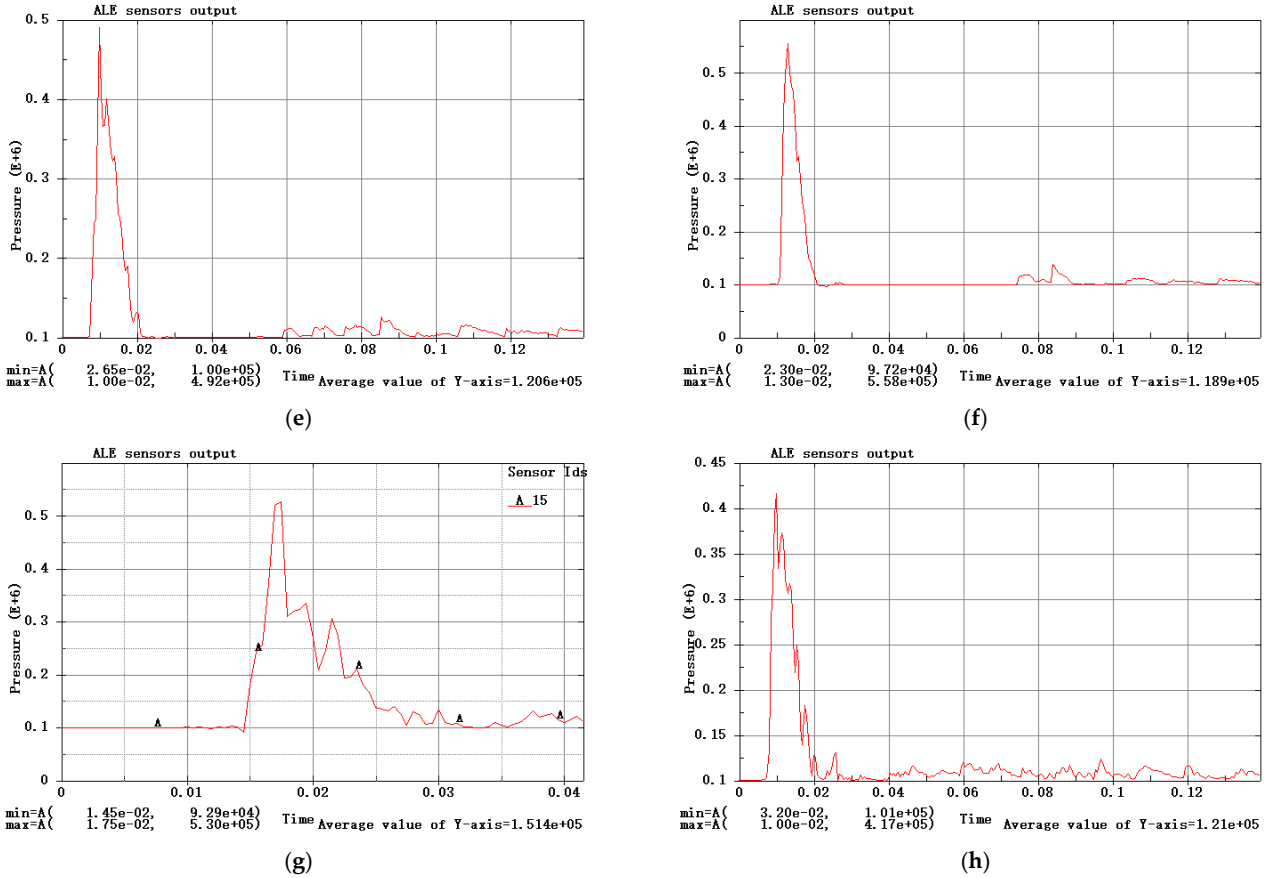

Figure 7. Time series of simulated slamming pressure in Case 4 of Model 1: (**a**) P1; (**b**) P2; (**c**) P3; (**d**) P4; (**e**) P5; (**f**) P6; (**g**) P7; (**h**) P8.

4. Comparison and Verification

This study mainly focuses on the plastic deformation and failure mechanism of structures. As the input for system response, the slamming pressure is the first to be measured. Therefore, the measured slamming pressure is selected to verify the reliability of the numerical and experimental results.

4.1. Convergence Study

To further verify the numerical simulation used in this work, it was necessary to conduct a convergence study. According to the methodology employed by Stern and Wilson [24], the convergence study of the grid is carried out in this section. Model 2 and Case 6 are selected, and the verification focuses on the slamming pressure of P2. In this study, four grid schemes, which are 80 mm × 80 mm, 40 mm × 40 mm, 20 mm × 20 mm, and 10 mm × 10 mm, respectively, were designed for the verification study.

The time series of the slamming pressure of P2 for the four grid systems were simulated and are shown in Figure 8. As can be seen, the overall trend of the slamming pressures obtained based on four grid schemes is similar, but the peak values differ significantly. The slamming pressure corresponding to the grid scheme of 80 mm × 80 mm is the lowest, and the slamming pressure increases with refinement of the mesh. The slamming pressure corresponding to the grid scheme of 20 mm × 20 mm is significantly higher than that of 40 mm × 40 mm, and the timing of peak occurrence is also different. In addition, when the mesh size is refined to 10 mm × 10 mm, the slamming pressure slightly increases, but the computation time significantly increases. Thus, to achieve a compromise between computation efficiency and accuracy, the grid scheme of 20 mm × 20 mm was selected for the subsequent simulation.

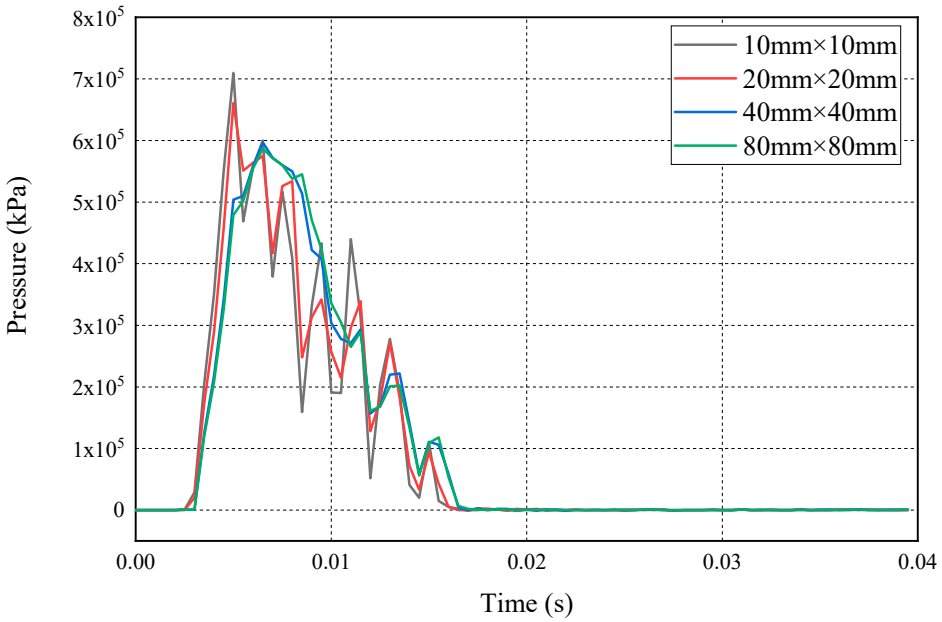

Figure 8. Time series of slamming pressure of P2 in Case 6 of Model 2.

4.2. Symmetry Verification

The time series of the slamming pressures at monitoring points P1 and P5 for Case 5 of Model 2 were simulated and are presented in Figure 9. It can be seen from Figure 6 that the same numbered points on #2 and #4 are symmetrically arranged. They enter the water simultaneously at the same height during the experiment, with P1 entering the water before P5.

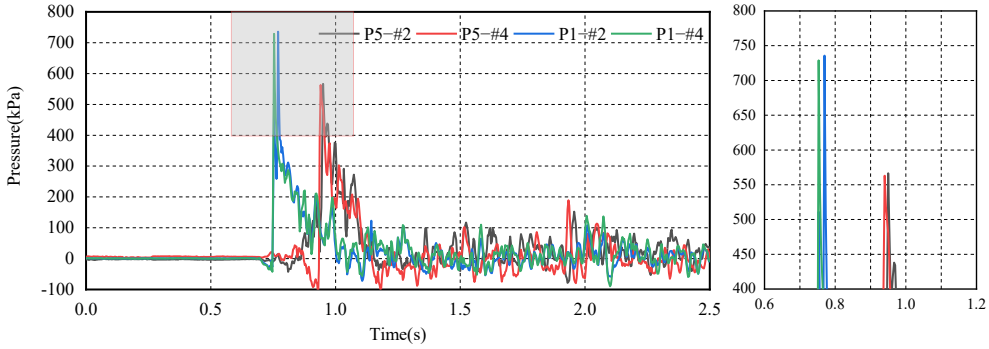

Figure 9. Time series of measured slamming pressure in Case 5 of Model 2.

As shown in Figure 9, the slamming pressure's time distribution resembles a pulse load pattern, with the pressure reaching its maximum at the moment of water entry and then decaying to zero. Since the pressure peak is proportional to the square of the water entry velocity, the same height results in the same water entry velocity, leading to nearly equal slamming pressure peaks at the same symmetric positions (P1-#2 and P1-#4; P5-#2 and P5-#4). This indicates that the physical process of slamming and the geometric shape of the model have good symmetry. The earlier water entry point reaches the pressure peak first. The earlier entry point has a higher pressure peak because it starts decelerating upon contact with the water. Furthermore, the entry point might have multiple peaks due to water splashing. The duration of the first peak is very short, which is followed by high-frequency oscillations. The times when the first peak appears, corresponding to the same height, are almost the same. The second peak of the time series has obvious randomness.

4.3. Independence of the Different Models

In this section, to verify the independence of the different test models, the experimental and simulation results of the slamming pressures of four stiffened plates at the same water entry velocity (10 m/s) are compared and presented in Figure 10. It can be seen that the test results for different stiffened plates at the same water entry velocity are not significantly different. This is because the slamming pressure peak only depends on the water entry velocity. Moreover, compared to the simulation results of different stiffened plates, the test results are slightly higher. The quantification of the deviation is presented in Table 3. As can be seen, deviations 1–4 denote the differences between the measured pressures of the four stiffened plates (#1−#4) and the simulation results, respectively. The maximum deviation occurs at P4 of stiffened plate #3, which is 10.36%, and the minimum deviation occurs at P7 of stiffened plate #4, which is 0.33%. It is found that the amount of deviation is relatively stable, proving the stability of the experimental measurements. Considering minor differences in instrumentation operation during each test, the experimental results are reliable.

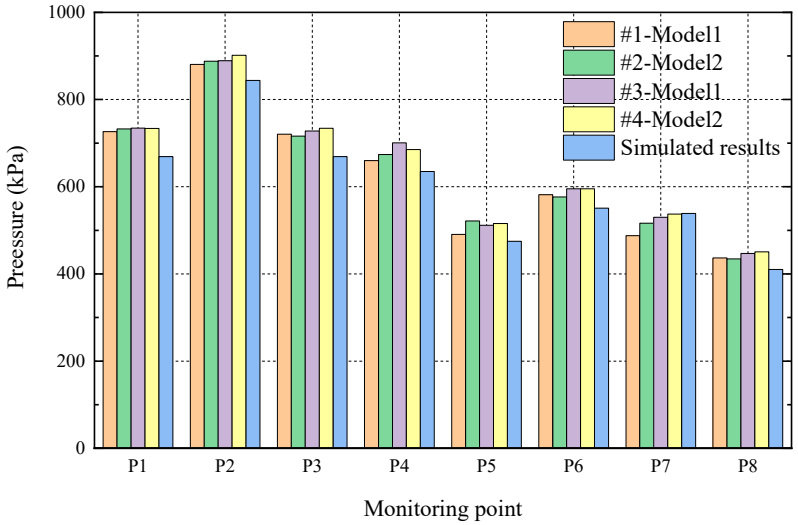

Figure 10. Comparison between measured pressure and simulated pressure.

Table 3. Quantification of the deviation in Figure 10 (kPa).

Point	#1-Model 1	#2-Model 2	#3-Model 1	#4-Model 2	Simulations	Deviation 1	Deviation 2	Deviation 3	Deviation 4
P1	726.28	732.76	734.53	733.76	669.00	8.56%	9.53%	9.79%	9.68%
P2	880.72	888.01	889.00	901.84	844.00	4.35%	5.21%	5.33%	6.85%
P3	720.69	716.19	727.97	734.07	669.00	7.73%	7.05%	8.82%	9.73%
P4	659.85	673.92	700.80	685.21	635.00	3.91%	6.13%	10.36%	7.91%
P5	490.66	521.66	511.55	515.64	475.00	3.30%	9.82%	7.69%	8.56%
P6	581.92	576.74	595.45	595.25	551.00	5.61%	4.67%	8.07%	8.03%
P7	487.62	516.41	529.82	537.20	539.00	9.53%	4.19%	1.70%	0.33%
P8	436.65	434.39	446.93	450.70	410.00	6.50%	5.95%	9.01%	9.93%

5. Results and Discussion

5.1. Distribution Pattern of Structural Strain

To meet the requirements of measurement accuracy, the microstrain was measured as the direct output by the strain gauges during the experiment. The time series of microstrain on the stiffened plates under Case-4 of Model 1 are presented in Figure 11. It is evident that the microstrain distribution over time is synchronized with the slamming pressure, occurring around 0.75 s. The plastic deformation can be seen from the time series of

microstrain. The spatial distribution of microstrain shows that the plastic microstrain on the stiffened panel is the highest, with the plastic microstrain reaching 8000 at point S16 and reaching 200,000 at point S18. The stiffened web takes second place, with the plastic microstrain ranging from 3000 to 6000, and the plastic microstrain of the plate grids being below 4000.

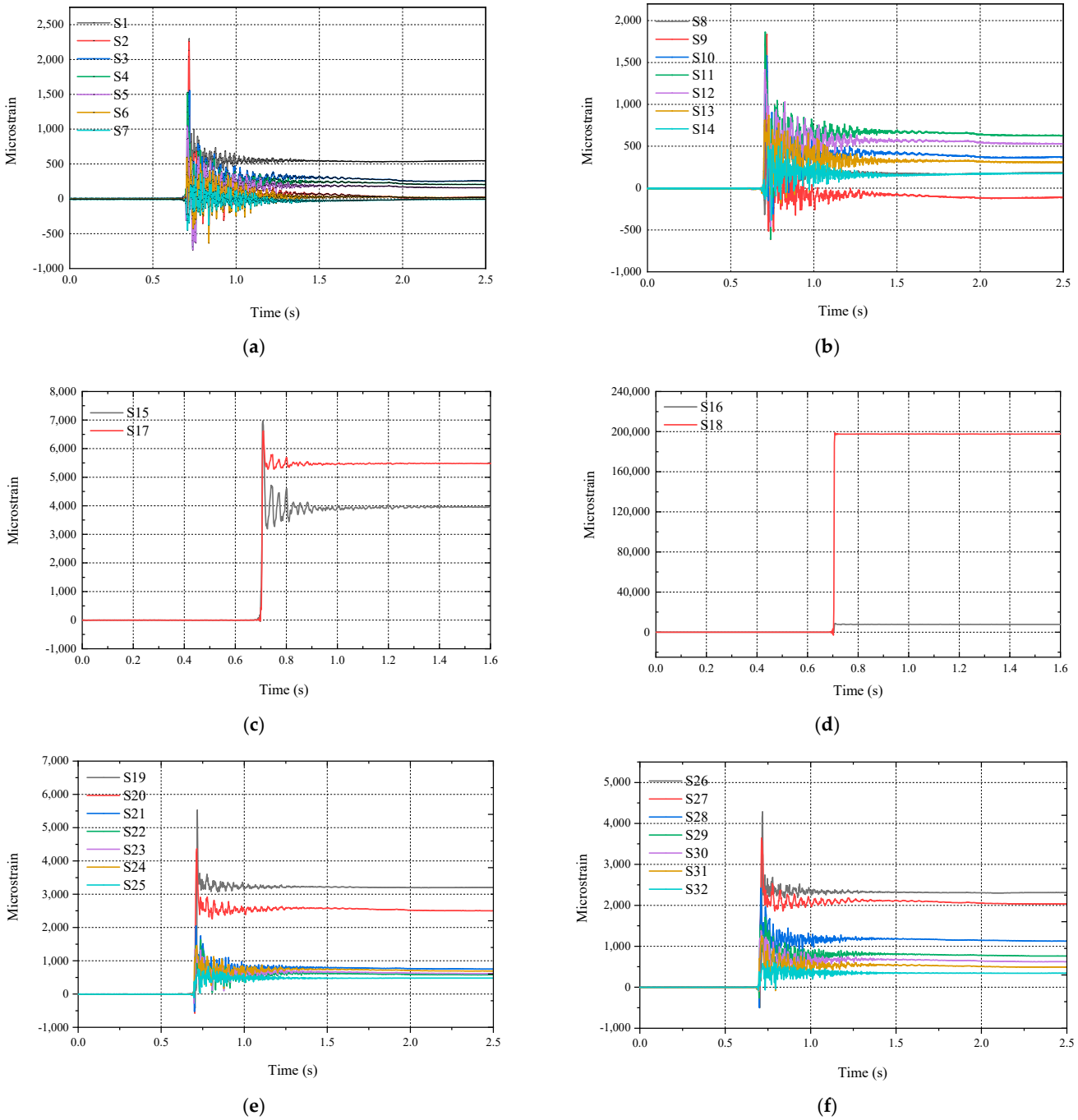

Figure 11. Time series of microstrain in Case 4: (**a**) S1–S7; (**b**) S8–S14; (**c**) S19–S25; (**d**) S26–S32; (**e**) S15 and S17 for web; (**f**) S16 and S18 for plate.

5.2. Analysis of Plastic Deformation of Stiffened Plates under Lateral Slamming Loads

From the time series in Figure 10, it is evident that the test models undergo plastic deformation under slamming loads. It is noted that the two models in each case can undergo varying degrees of plastic deformation, but the cases under which full plastic

deformation occurs differ between the two stiffened plate models. The stiffened plate with angled steel (Model 1) undergoes plastic deformation at the water entry velocity of 10 m/s (Case 4), while the stiffened plate with a T-section stiffener (Model 2) undergoes plastic deformation at the water entry velocity of 12 m/s (Case 6). The post-test deformations of the stiffened plates are shown in Figure 12.

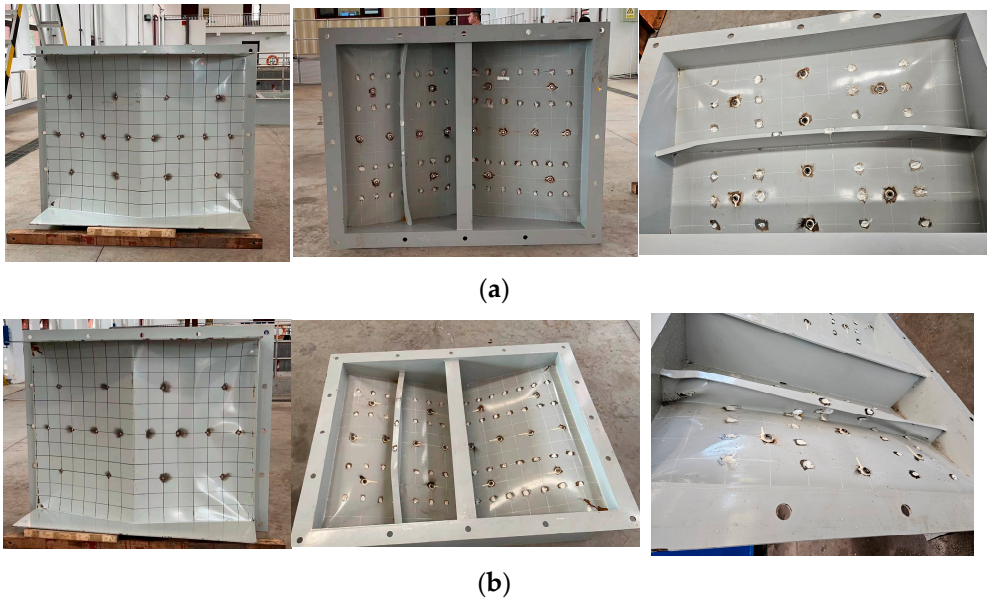

(**a**)

(**b**)

Figure 12. Plastic deformation of the two models: (**a**) Model 1 (Case 4); (**b**) Model 2 (Case 6).

As shown in Figure 12, both models exhibit extensive plastic deformation, with damage to the plate grids, stiffened panels, and stiffened webs. This indicates that the dynamic ultimate strength failure test of stiffened plates under lateral slamming loads is completed in the study. As shown in Figure 12a, the plastic deformation in the middle of the plate grid and along the diagonal is significant, leading to a half-inverted roof shape. As shown in Figure 12b, the failure mode of the plate grid of Model 2 is the formation of plastic hinges along the diagonal of the plate edge, with concave deformation occurring in the middle of the plate grid. The failure mode of the stiffener is the formation of plastic hinges at the ends (boundaries) of both the web and panel, causing lateral deformation of the stiffener.

To more intuitively observe the deformation of the stiffened plates after testing, scanning measurements were conducted on the stiffened plate components under various conditions. The structural deformation measurements of each component after the test are presented in Figures 13 and 14. As shown in Figures 13 and 14, the deformation of the non-stiffened plate exhibits a symmetrical shape, while the stiffened plate exhibits an asymmetrical shape, with the deformation of the plate being greater than that of the stiffened plate, indicating that stiffening enhances the resistance to deformation. Moreover, it is noted that although the maximum deformations of the stiffened plate and stiffener in Case 6 are slightly larger than those in Case 4, the water entry velocity of Model 2 with full plastic deformation is greater. Thus, the T-section stiffener has stronger resistance to deformation under slamming loads.

Finally, the deformation trends of different components in each model after testing are presented in Figure 15. It can be seen that the overall deformation for different components in each model increases with increasing water entry velocity (drop height). Furthermore, the plate grid deformation and stiffener deformation of the T-section stiffened plate are smaller than those of the angled steel stiffened plate under the same water entry velocity, indicating that the T-section stiffener has a stronger ability to resist plastic deformation under slamming loads.

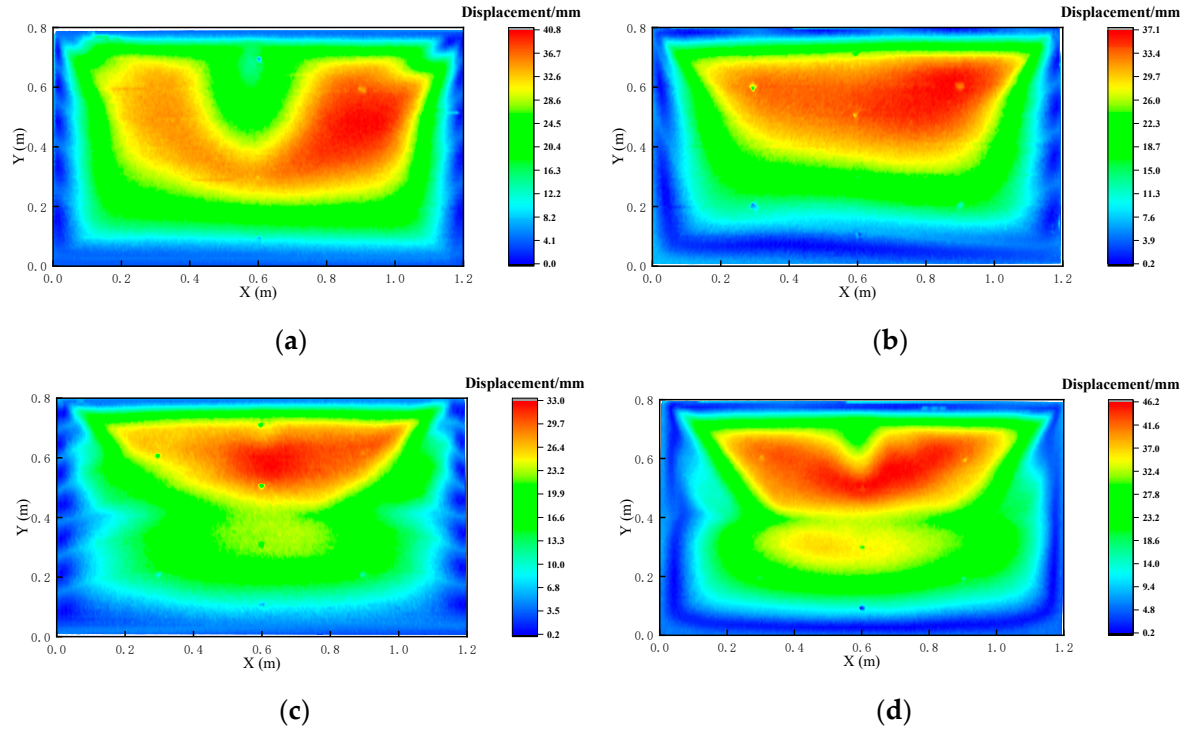

Figure 13. Deformation of plates: (**a**) #1 (Case 4); (**b**)#2 (Case 6); (**c**) #3 (Case 4); (**d**) #4 (Case 6).

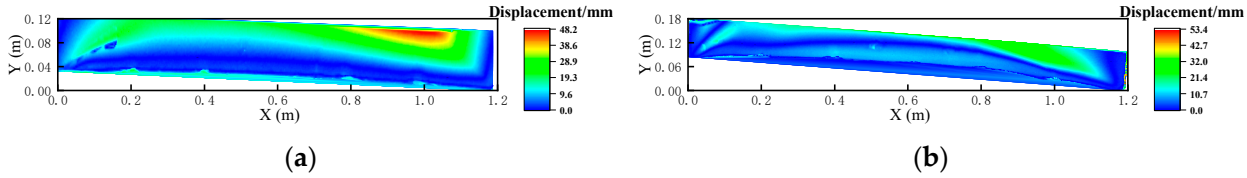

Figure 14. Deformation of stiffeners: (**a**) Angled steel; (**b**) T-section steel.

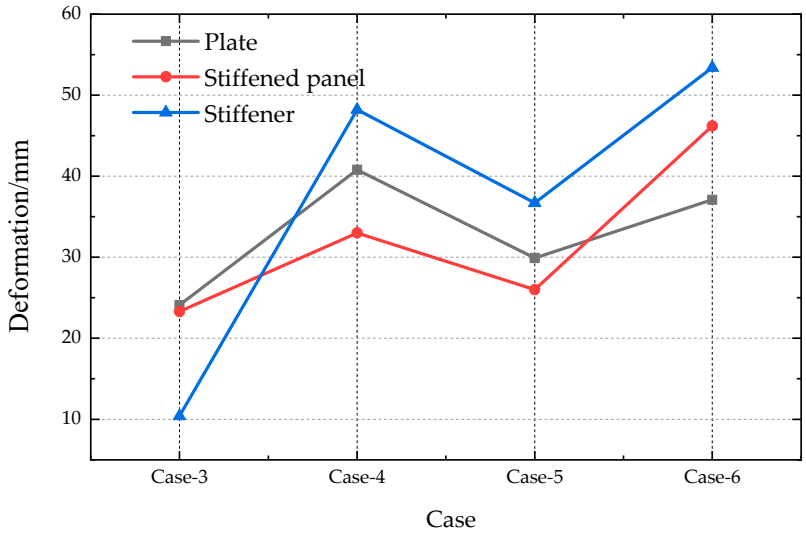

Figure 15. Deformation trend of different members after each model test.

6. Conclusions

By using numerical simulations based on LS-DYNA software (LS-DYNA_mpp_s_R11_0) and free-drop slamming tests, the dynamic ultimate bearing capacity of the structure under lateral slamming loads, including structural strain and plastic deformation, was analyzed

for stiffened plates with different stiffnesses. The focus of the study was on analyzing the influence of factors such as different stiffness, position, and water entry velocity on the plastic deformation of the structure. The following conclusions can be drawn:

(1) The time distribution pattern of slamming pressure resembles a pulse load, with the pressure reaching its maximum at the moment of water entry. The spatial distribution of slamming pressure is related to the order of water entry. Points entering the water simultaneously at the same vertical height have similar peaks of slamming pressure, with earlier entry points experiencing higher peak pressures. Points entering later may have multiple peaks due to splashing water.
(2) The time series of microstrain is synchronized with the slamming pressure, and plastic deformation occurs in the structure. The spatial distribution shows that the plastic deformation on the stiffened panel is the highest.
(3) Under slamming loads, the failure mode of the plate and stiffened plate grids involves the formation of plastic hinges along the plate edge diagonals, with concave deformation occurring in the middle of the plate grids. The failure mode of the stiffener involves the formation of plastic hinges at the ends (boundaries) first, followed by stiffener lateral deformation.
(4) Stiffeners can enhance the ability of stiffened plates to resist plastic deformation under slamming loads, with T-section stiffeners providing stronger resistance to plastic deformation. Increasing the plate thickness can improve the ability to resist plastic deformation.

It is noted that the water entry angle of 15° was selected in this study based on past experimental experience, and the influence of the water entry angle on the slamming pressure and structural response characteristics needs be determined. Thus, free-drop experiments of models with different water entry angles will be conducted in the future.

Author Contributions: Conceptualization, J.X. and Z.C.; methodology, J.X.; software, Z.C. and W.Z.; validation, J.X., Z.C. and W.Z.; formal analysis, S.C.; investigation, Z.C.; resources, J.X.; data curation, N.Z. and S.C.; writing—original draft preparation, Z.C. and Q.T.; writing—review and editing, Z.C. and Q.T.; visualization, W.Z.; supervision, J.X. and N.Z.; project administration, J.X. and S.C.; funding acquisition, J.X. and Z.C. All authors have read and agreed to the published version of the manuscript.

Funding: This research was funded by the State Key Laboratory of Structural Analysis, Optimization and CAE Software for Industrial Equipment, Dalian University of Technology (Grant number GZ23112 and GZ23109). The APC was funded by the China Ship Scientific Research Center, Wuxi.

Institutional Review Board Statement: Not applicable.

Informed Consent Statement: Not applicable.

Data Availability Statement: All data, models, or code generated or used during the study are available from the corresponding author by request.

Conflicts of Interest: The authors declared that they have no conflicts of interest to this work.

References

1. AbuBakar, A.; Dow, R.S. Simulation of ship grounding damage using the finite element method. *Int. J. Solids Struct.* **2013**, *50*, 623–636. [CrossRef]
2. Ehlers, S. The influence of the material relation on the accuracy of collision simulations. *Mar. Struct.* **2010**, *23*, 462–474. [CrossRef]
3. Liu, B.; Pedersen, P.T.; Zhu, L.; Zhang, S. Review of experiments and calculation procedures for ship collision and grounding damage. *Mar. Struct.* **2018**, *59*, 105–121. [CrossRef]
4. Howison, S.D.; Ockendon, J.R.; Wilson, S.K. Incompressible water entry problems at small deadrise angles. *J. Fluid Mech.* **1991**, *222*, 215–230. [CrossRef]
5. Stenius, I.; Rosén, A.; Kuttenkeuler, J. Explicit FE-Modelling of Fluid-Structure Interaction in Hull-Water Impacts. *Int. Shipbuild. Prog.* **2006**, *53*, 103–121.
6. Ren, H.; Yu, P.; Wang, Q.; Li, H. Dynamic response of the bow flare structure under slamming loads. In Proceedings of the 34th International Conference on Ocean, Offshore and Arctic Engineering (ASME 2015), St. John's, NL, Canada, 31 May–5 June 2015.

7. Iijima, K.; Fujikubo, M. Hydro-elastoplastic behaviour of VLFS under extreme vertical bending moment by segmented beam approach. *Mar. Struct.* **2018**, *57*, 1–17. [CrossRef]
8. Yang, L.; Peng, Z.L.; Wang, D.Y. Experimental and numerical investigation of material failure criterion with high-strength hull steel under biaxial stress. *Ocean Eng.* **2018**, *155*, 24–41. [CrossRef]
9. Yang, B.; Soares, C.G.; Wang, D.Y. Dynamic ultimate compressive strength of simply supported rectangular plates under impact loading. *Mar. Struct.* **2019**, *66*, 258–271. [CrossRef]
10. Yang, B.; Wang, D. Buckling strength of rectangular plates with elastically restrained edges subjected to in-plane impact loading. *Proc. Inst. Mech. Eng. Part C J. Mech. Eng. Sci.* **2017**, *231*, 3743–3752. [CrossRef]
11. Zhu, S.J.; Wu, M.K.; Moan, T. Experimental investigation of hull girder vibrations of a flexible backbone model in bending and torsion. *Appl. Ocean Res.* **2011**, *33*, 252–274. [CrossRef]
12. Stenius, I.; Rosén, A.; Battley, M.; Allen, T. Experimental hydroelastic characterization of slamming loaded marine panels. *Ocean Eng.* **2013**, *74*, 1–15. [CrossRef]
13. Chen, Z.Y.; Jiao, J.L.; Li, H. Time-domain numerical and segmented ship model experimental analyses of hydroelastic responses of a large container ship in oblique regular waves. *Appl. Ocean Res.* **2017**, *67*, 78–93. [CrossRef]
14. Chen, Z.Y.; Gui, H.B. Research on Whipping and Springing Responses of Hull based on Different Experimental Method and Nonlinear Hydroelastic Time-domain Theory. *J. Ship Mech.* **2017**, *21*, 1143–1158.
15. Luo, H.; Liu, X.; Dong, D.; Zhao, Z.; Ji, H.; Gao, Y.; Lin, W. Experimental investigation of water impact of one free-drop wedge with stiffened aluminum panels. *Chin. J. Hydrodyn.* **2014**, *29*, 460–468.
16. Si, H.L.; Zhao, N.; Hu, J.J. Experimental study of slamming loads on ship bow during free water entry. *J. Ship Mech.* **2020**, *24*, 445–455.
17. Mo, L.X.; Wang, H.; Jiang, C.X.; Xu, C. Study on dropping test of wedge grillages with various types of stiffeness. *J. Ship Mech.* **2011**, *15*, 394–401.
18. Chen, X.P.; Li, J.W.; Wang, H.; Qi, E.R. Experiments and numerical investigation of water entry of large-scale steel wedge models. *J. Ship Mech.* **2012**, *16*, 1152–1163.
19. Wang, Q.; Yu, P.Y.; Fan, G.J.; Li, G.Z. Experimental drop test investigation into cross deck slamming loads on a trimaran. *Ocean Eng.* **2021**, *240*, 109999. [CrossRef]
20. Li, H.; Deng, B.L.; Zou, J.; Dong, C.R.; Liu, C.L.; Liu, P.L. Experimental free-drop test investigation into wet-deck slamming loads on a generic trimaran section considering the influence of main hull profile. *Ocean Eng.* **2021**, *242*, 110114. [CrossRef]
21. Duan, W.Y.; Liu, J.Y.; Liao, K.P.; Ma, S. Experimental study of slamming pressure for a trimaran section with different drop heights and heel angles. *Ocean Eng.* **2022**, *263*, 112400. [CrossRef]
22. Stavovy, A.B.; Chuang, S.L. Analititcal determination of slamming pressure for hign speed vehicals in waves. *J. Ship Res.* **1976**, *20*, 190–198. [CrossRef]
23. Ochi, M.D.; Bonilla-Norat, J. *Pressure-Velocity Relationship in Impact of a Ship Model Dropped onto the Water Surface and in Slamming in Waves*; AD-709071; National Academy of Sciences: Washington, DC, USA, 1970.
24. Stern, F.; Wilson, R.V.; Coleman, H.W.; Paterson, E.G. Comprehensive approach to verification and validation of CFD simulations—Part 1: Methodology and procedures. *J. Fluids Eng.* **2001**, *123*, 793–802. [CrossRef]

Disclaimer/Publisher's Note: The statements, opinions and data contained in all publications are solely those of the individual author(s) and contributor(s) and not of MDPI and/or the editor(s). MDPI and/or the editor(s) disclaim responsibility for any injury to people or property resulting from any ideas, methods, instructions or products referred to in the content.